New developments in magnetic gradiometry

Ronny Stolz[1], Anre Vorster[2], Vyascheslav Zakosarenko[1,3], Matthias Schmelz[1], Markus Schiffler[1,4], Thomas Schoenau[1], Matthias Queitsch[3,4], Andreas Chwala[1], Matthias Meyer[3], Louis Polomé[5], Hans-Georg Meyer[1]

1. Leibniz Institute of Photonic Technology, Jena, Germany
2. De Beers Exploration, Johannesburg, Republic of South Africa
3. Supracon AG, Jena, Germany
4. Institute of Geoscience, Friedrich Schiller University, Jena, Germany
5. Spectrem Air Ltd., Johannesburg, Republic of South Africa

ABSTRACT

Vector magnetometry in surveys for mineral exploration remains a challenge even with the highly sensitive magnetic field sensors that are currently available. Highly sensitive magnetometers such as Superconducting QUantum Interference Devices (SQUIDs) in mobile operation place a strong demand on the required dynamic range of the data acquisition system as it easily exceeds 24 bits. One solution to overcome this hurdle is to acquire gradiometry data. With this method, the spatial derivatives of the magnetic field vector, also called the magnetic gradient tensor, are measured.

In this review, various sensor technologies are introduced, which allow for the design of sensors that measure individual magnetic gradient components. These sensors are called gradiometers and provide better information if the full gradient tensor is mapped during mineral exploration applications. There are already a number of full tensor magnetic gradiometers on the market which measure all components of the magnetic gradient. They are applied in mineral exploration, detection of UXO, and archaeology.

The main focus of this work is on SQUID based gradiometry which enables the measurement of very weak magnetic gradients within the Earth's magnetic field. Due to their ability to suppress a homogeneous magnetic field, the demands in terms of motion noise and dynamic range for field operation are relaxed compared to vector magnetometers. Using superconducting technologies various concepts for building gradiometers are available. Herein, low temperature superconducting planar-type first-order gradiometers will be introduced. They are 6 cm x 2 cm in size and have intrinsic noise floors of better than 50 fT/(m√Hz) down to 0.3 Hz. The highly symmetric SQUID gradiometers presented herein reduce the homogeneous part of the Earth's field by at least a factor of 5,000. If the signals of a triple reference magnetometer are used, this homogeneous magnetic field is further reduced by a factor of better than 10^7 by using appropriate software algorithms.

Full tensor measuring instruments were built using these gradiometers. They proved to be mechanically robust, reliable with low power consumption, easy to maintain and airworthy. The results of a test survey flown with the SQUID gradiometers are presented here and allow for a preliminary assessment of the exceptional performance of SQUID based full tensor gradiometry.

Taking advantage of the unique properties of SQUIDs, in particular their periodic flux to voltage characteristics, enables new approaches for high-resolution vector magnetometers that are suitable for magnetic methods. Example developments will be introduced.

INTRODUCTION

Surveying the Earth's subsurface using magnetic field sensors is one of the oldest and most often used techniques in mineral exploration. It is a relatively easy to apply and an inexpensive tool to study properties of the rock materials in the Earth crust up to the uppermost meter of soil. There is a variety of literature and reviews available which describe the method, the data acquisitioning and processing, the transformations between magnetic properties as well as inversion and interpretation techniques [1] or more with focus on mineral exploration by [2], [3], or [4].

The magnetic method is utilized in all environments: ground-based, downhole, marine, submarine and airborne. But, very importantly, it is used in airborne mineral exploration. Surveying is a search for local perturbations in the Earth's magnetic field which represent a sufficient contrast of the magnetization of different rock materials. The anomalies are caused by magnetized geological features such as mineral deposits, geological structures; buried engineering features e.g. mineshafts, sink holes, pipes, unexploded ordnances (UXOs) or archaeological remainders. The focus of this work is on airborne mineral exploration which is relatively fast and simple as well as inexpensive compared to most other geophysical methods. Magnetic observations are done e.g. on a regular base in mineral exploration even in remote areas and regions with limited access.

The first section will formulate the problem in airborne magnetics which will be followed by a short review of available sensor technologies. The subsequent section will introduce our full tensor magnetic gradiometer (FTMG) system, which is based on hardware first-order planar-type SQUID gradiometers. Section

three will discuss recent progress in data processing, inversion and interpretation. Subsequently, a field survey example with the FTMG instrument will be presented.

MAGNETIC FIELD SENSORS

The history of magnetic field detectors dates back to ancient Greece and later China (500 years BC) with the various magnetic compass types. The compass was first used in Italy as tool for mining in the 13 to the 14th century [5]. Later, up to about World War II, pivoted needle instruments or magnetic variometers were mainly used for magnetic observations [2]. In 1937 Friedrich Foerster developed the first fluxgate sensors which could be used to measure all three components of the Earth's magnetic field induction vector abbreviated herein as magnetic field vector. This enabled the first industrial wide use of magnetic field sensors, so called magnetometers, for mineral exploration. The interested reader is referred to [6] for an overview on the history and for a general overview and new developments of fluxgate sensors to e.g. [7–9], respectively.

Today there are a large variety of magnetic field sensors in general, refer to [10] or [11], and for geophysical applications these include induction coils (e.g. [12]), fluxgates, resonance magnetometers and Superconducting Quantum Interference Detectors (SQUIDs). In the subsequent section the operation of SQUIDs will be introduced since they are of particular importance for this review.

Although Giant magnetoresistance (GMR) type sensors gained importance in some geo-engineering applications such as solid soil analysis or the search for UXO's, they are not relevant for this work and will thus not be included.

All vector-type magnetic field sensors such as fluxgates suffer from a general problem – the more sensitive they get, the higher is the required dynamic range¿). For analogue to digital converters (ADCs) this property is comparable to the given signal-to-noise-ratio SNR. Herein according to [13], we define this property by the relation

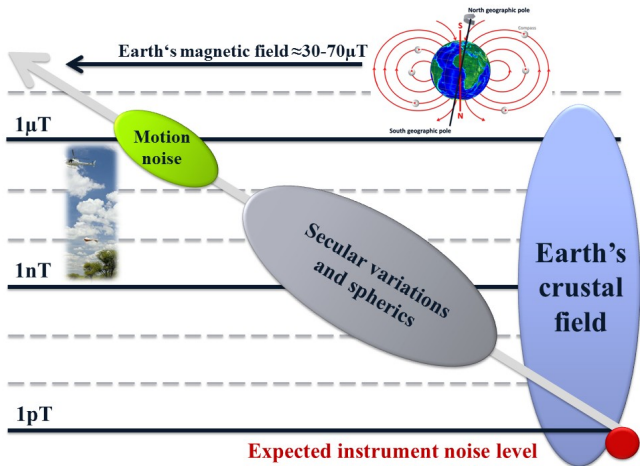

Figure 1: Illustration of the required dynamic range for magnetometers in airborne operation for mineral exploration.

$$DNR = 20\,dB \cdot \log_{10}\left(\frac{B_{max}/\sqrt{Hz}}{B_N}\right) \qquad (1)$$

with B_{max} and B_N being the full-scale output and the noise level in the bandwidth of $1\,Hz$ for the according magnetic field sensor instrument [14, 15], respectively. Let's consider the measurement of the vector components of the magnetic field in mobile operation: if one assumes amplitude changes of more than $50\,\mu T$ for the magnetometer in operation, the required field resolution of about $1\,pT$ equals according to eq. (1) a dynamic range exceeding $154\,dB$. This corresponds to $25.6\,bit$ noise-free resolution of the magnetic field. Only a sensor system with a DNR of this range would be able to detect subtle magnetic anomalies when it is rotated in the Earth's magnetic field vector during survey operation. But, at present, the best commercial sensors are only 24 bit ADCs with less than 24 bit noise-free resolution. The signal ranges for airborne operation of magnetometers are illustrated in Fig.1.

With only 8 bit ADCs available in the mid 1950's, vector-type magnetometers, like fluxgates, were difficult to implement into exploration instruments since their sensitivity for rotations and hence huge DNR. In order to overcome this limitation, two solutions were put into effect: total field sensors and gradient sensors, so called gradiometers:

1) Total field magnetometers

This type of magnetometers does not measure components of the magnetic induction vector but its absolute value $|\vec{B}|$ which is also called the total magnetic field intensity TMI. Typically by subtracting the mean value from a reference field B_0, e.g. the International Geomagnetic Reference Field (IGRF) [16] or the High Definition Geomagnetic Model (HDGM) [17], the local anomalous field $|\vec{B}| - B_0$ called total field anomaly (TFA) is obtained. Since the TMI is rotationally invariant, the dynamic range is fairly reduced in mobile operation. Today, state of the art TMI magnetometers in airborne magnetic exploration are nuclear resonance magnetometers like proton-precession, alkali-vapor, and Overhauser instruments [3, 4]. They are commercially available through various suppliers e.g. Scintrex, Geometrix, GEM Systems and Polatomic. The CS-3 [18] of Scintrex Ltd. as a typical example provides a portable magnetometer with operating range between $15\ldots105\,\mu T$ with noise envelope of $2\,pT_{pp}$ in $0.1\,Hz$ bandwidth.

However, TMI magnetometers have various shortcomings:

- the TMI measurements is not a true potential field like the magnetic field vector,
- no directional information is available,
- dead zones and directional errors like $\Delta|\vec{B}| \approx 0.2\,nT$ for Scintrex's CS-3, for example.

New types of optical magnetometers are evolving with the aim of achieving a range of magnetic field sensitivities which were to date have been only accessible by SQUIDs. Budker et al. [19] summarize most of the new sensor developments like Spin-

Exchange-Free (SERF), nitrogen-vacancy centers in diamond (NVCD), cold atom magnetometers and others in their exhaustive review. Already, shot-noise limited magnetic field resolutions in the range of $1 fT/\sqrt{Hz}$ e.g. in [20] were achieved for active cell volumes of about $100\,mm^3$ and recently $0.1 fT/\sqrt{Hz}$ in a second reading time [21] with magnetometers working in SERF mode. But, these magnetometers only work in extremely low ambient magnetic field and are unusable in the Earth field. Our approach with the light-shift dispersed Mz (LSD-Mz) readout mode of the optically-pumped alkali magnetometer (OPM) can operate in the ambient Earth magnetic field and will result in a field resolution of the order of $10 fT/\sqrt{Hz}$ [22] and is thus a very promising candidate especially for magnetic exploration. Also NVCDs and cold atoms are well-suited to build high sensitive magnetometers in future. But, so far the presented sensitivities are not sufficient.

2) Gradiometers

Since the Earth's magnetic field without magnetic anomalies in the crust is homogeneous on scales of the order of tens of kilometers, the measurement of the first-order spatial derivatives of the magnetic field, the first-order magnetic field gradient, strongly reduces the required DNR. In general there are nine separate components $\partial B_i/\partial x_k = B_{ik}$ of the gradient, also called gradient tensor, which have to be measured by gradiometers. Not all tensor components are independent from each other. With ¿ $\vec{B}=0$ and by assuming a quasi-stationary magnetic field for most scenarios in geomagnetics which leads to $curl\,\vec{B}=0$, the first-order magnetic gradient tensor (MGT) has only five linear independent components; for example the set $\left(B_{xx}, B_{xy}, B_{xz}, B_{yy}, B_{yz}\right)$ which need to be measured. The gradient tensor measured at one location carries knowledge about magnetic sources, which contain significantly more information than the magnetic field vector which in turn is better than the TMI. However, the strength of the magnetic gradient signal for typical geomagnetic scenarios diminishes faster with distance than does the magnetic field signal. Thus, the typical depth of exploration for a gradient sensor is lower than for magnetic field observations. For an ideal magnetic dipole target with magnetic moment of $m=|\vec{m}|$ at a distance of r to the sensors, the scaling rule is m/r^3 and m/r^4 for the magnetic field and gradient measurement, respectively.

The use of gradiometers provides on the other hand various advantages. A review on those is provided in [23]. Some of the important advantages are:

- gradiometers are less sensitive to rotations in homogeneous magnetic field and thus reduce DNR dramatically,
- gradiometers suppress the homogeneous magnetic field and do not suffer from geomagnetic noise,
- long wavelength regional trends in the gradient signals are removed,
- spatial resolution of gradient tensor data is in theory higher by a factor of two [24],
- the data provides additional information for the identification of magnetic remanence indicators,
- improved interpretation of gradient tensor data on irregular grids [25],
- gradient tensor data provide significant constraints to the solution of the inverse problem, e.g., the dipole-tracking algorithm [26] and have been successfully applied to estimate the location of block-shaped bodies.

The next section will review in detail the available solutions to build magnetic gradiometers.

MAGNETIC GRADIOMETRY

Gradiometers are very popular because of their ability to suppress environmental noise from distant sources, and are used extensively in biomedical imaging and the non-destructive testing of materials. There are a variety of magnetic gradiometers available. In this work only sensors for first-order gradients are considered which will be distinguished by their specific construction:

1) Software gradiometers

The most common way to build a first-order gradiometer is to use two magnetometers and to subtract their output signals either electronically or in software. The two sensors with a pickup area $\vec{A}_i$ are placed at different locations. The separation of the two sensors is given by the baseline $b=|\vec{b}|$. The first proposals for an airborne magnetic gradiometer system were made by Fromm [27]. He suggested that the gradiometer could be constructed from two magnetic sensors either connected in parallel in a rigid frame or both independently stabilized so that their sensitive axes remain parallel. Since the sensors operate in the Earth's magnetic field during airborne surveys, exceptional high dynamic range is required to ensure low noise performance. There have been many attempts using vector-type magnetometers like fluxgates, e.g. [28–31] or others. But, these gradiometers are critical to calibrate in order to reduce noise arising from non-orthogonality, scaling, and misalignment errors of the three magnetometers, directional dependence of sensitivity of the magnetometers, nonlinearities from sensors and electronics, and cross talk. For marine applications new instruments deploying Overhauser and vector magnetometers were simultaneously developed [32]. Using a very long baseline of about $150\,m$, a combined highly sensitive vector magnetometer/gradiometer was built.

In view of this problem the TMI magnetometers became very attractive in exploration in the 1960's since they are relatively insensitive against angular rotations of the sensor in the Earth's magnetic field. An initial report on a first-order horizontal derivative gradiometer built with two OPMs (optically pumped magnetometers) in airborne magnetic surveys is given in [33]. Nowadays, a variety of different platforms and ***total field gradiometer*** configurations using OPM are available [34]:

- vertical gradiometers which resolve near surface magnetic sources better than TMI magnetometers,
- horizontal gradiometers, which were introduced by Geometrics in 1983 and provide also detailed near-surface information, but can also be used for enhanced interpolation

between flight lines, which is important if the magnetic anomaly signature has dimensions similar or smaller than the line spacing, or
- the 3-axis type introduced by Geodass in the 1990's as a combination of vertical and horizontal gradiometers.

Typical resolution between $1\,pT_{pp}$ and $20\,pT_{pp}$ are achieved for a single sensor. But often, the comparison of the gradiometer baseline to the sensor-to-source-distance r is not taken into account: If the baseline length b is comparable to r, the output signal of the software gradiometer corresponds not to a gradient B_{ik}. It is just a difference in the magnetic field at the two sensor locations $B_1 - B_2$. For example, a horizontal sensor arrangement like wing-tip or boom configurations such as the MIDAS instrument with baselines exceeding $15\,m$ are sensors measuring the difference in magnetic field, also called pseudo-gradient sensors, when the distance to the source is about $r < 5 \cdot b$ as a rule of thumb for a far-field approximation.

The measurement of the total field gradient with alkali vapour magnetometers is currently the most commonly used method in airborne magnetic surveys because of their simple operation. These instruments will be of especial interest again, if more sensitive OPMs enter the market.

An elegant solution for using high-sensitive vector-type magnetometers to build axial gradiometers for the on-diagonal gradient tensor components $B_{ii}\left(i \in x, y, z\right)$ is to form a three sensor gradiometer: Two high sensitive sensors form the gradiometer. A third less sensitive magnetometer is used to measure the homogeneous magnetic field with lower DNR and is coupled back to the first two. Thus, the signal of the less sensitive magnetometer, and its noise, is cancelled by calculating the difference signal of the sensitive magnetometers. This proposal of a three SQUID gradiometer (TSG) was developed by Koch et al. [35].

This TSG approach was later extended by a global feedback scheme [36]. Thereby, a three axis Helmholtz coil system is controlled by three reference magnetometers to compensate for the homogeneous Earth's magnetic field. Pairs of sensitive magnetometers in the center of the Helmholtz coil arrangement form the gradiometers. They operate in a residual magnetic field during mobile operation which reduces the demand on the dynamic range. As long as the feedback circuit, which involves the Helmholtz coils and reference magnetometers, produces a sufficiently homogeneous magnetic reference field, the homogeneity of the field is sufficient, and the gradiometer is working properly, the signal difference of the magnetometer pairs measures the gradient and no noise is caused by the reference magnetometer signals.

There exists an option to use sensitive SQUID based magnetometers in mobile operation for building software gradiometers, if specific SQUID readout schemes are used which provide a huge DNR. One example is for instance the flux-counting readout electronics [37–39] which allows for high resolution observations as long as the periodic SQUID characteristic is not compromised. A description of SQUID's and their characteristics can be found in the subsequent section.

The required dynamic range can also be reduced if lower instruments sensitivity is acceptable. This approach is used for instance by the T877 gradiometer of Tristan Technologies [40].

Another variant of CSIRO (Australia) adapts the idea of former gravity gradiometer instruments e.g. by Lockheed Martin: a sensitive magnetometer or a first-order axial gradiometer is rotated in the Earth's magnetic field [41, 42]. The latest approach of the rotating magnetic tensor gradiometer consists of an approximately axial or transverse gradiometer rotating about a perpendicular axis which separates gradient components in the frequency domain and enables absolute-value measurements of all components of the first-order MGT. Three of these rotating drums are required to determine the whole MGT. Initial results from an instrument called GETMAG in mineral and oil exploration have been shown [43].

In future, the new OPM sensors will enable the use of two smaller sensor elements with sufficient sensitivity to build software gradiometers. SERF-OPM gradiometers have already been characterized for biomagnetic applications with a sensitivity of about ¿ $280\,fT/\left(m \cdot \sqrt{Hz}\right)$ [44]. But, this development has not yet been completed or demonstrated in the Earth's magnetic field. There are expected to be new readout schemes that allow in future for highly sensitive gradiometers implemented on-chip.

There is a lot of R&D work going on in NVCD magnetometers and various readout schemes. For instance for laser threshold magnetometry a sensitivity of about ¿ $2\,fT/\sqrt{Hz}$ can be achieved for a $1\,mm^3$ diamond which will be $1{,}000$ times better than current NVCD demonstrations [45, 45, 45] in low magnetic fields. More realistically for smaller diamonds with diameter of about $100\,\mu m$ size a sensitivity of about $100\,fT/\sqrt{Hz}$ [46] could be reached. The first implementations of gradiometry [47, 48] are also shown.
The first implementation of FTMG using Ramsey type interferometry on cold atoms have already been demonstrated [49] with errors of ¿ $2.5(7)\,nT/mm$.
Naturally, there are still many improvements required for these new sensor technologies to build field-worthy instruments.

2) Hardware or intrinsic gradiometers
This type of gradiometer is a single sensor measuring the difference of the magnetic field at two different locations directly.

So far only two approaches were successfully undertaken:

- vibrating string gradiometer [50, 51] with sensitivities of the order of $10\,pT/\left(m \cdot \sqrt{Hz}\right)$; the isolation from vibrations and thermal influence is the main issue with this type of sensor,
- SQUID based wire-wound or on-chip gradiometers.

SQUID based gradiometers have successfully demonstrated their use in mineral exploration. Therefore, the sensor technology, important parameters, instruments, data processing and examples will be presented in the subsequent section of this work.

SQUID BASED FULL TENSOR GRADIOMETRY

SQUIDs

In this work, only a short overview on SQUIDs will be given. For an in-depth understanding of superconductivity and its various effects please refer to the excellent textbooks e.g. [52]. A detailed theory on SQUIDs and their operation can be found e.g. in [53]. The application of SQUIDs for instance as high sensitive magnetometers is described in [9, 54].

The instrument which will be presented herein uses dc SQUIDs [55] which make use of a superconducting (sc) loop interrupted by two weak links, the blue sections in Fig. 2 which are called Josephson junctions. In general dc SQUIDs, as depicted in Fig. 2, make use of:

- the Meissner-Ochsenfeld effect: expulsion of a magnetic field from a superconductor,
- cryo-cooled superconducting rings; for instance of low-temperature superconductors (LTS) e.g. niobium at boiling temperature of liquid helium $4.2\,K$ or of high-temperature superconductors (HTS) at boiling temperature of liquid nitrogen $77\,K$;

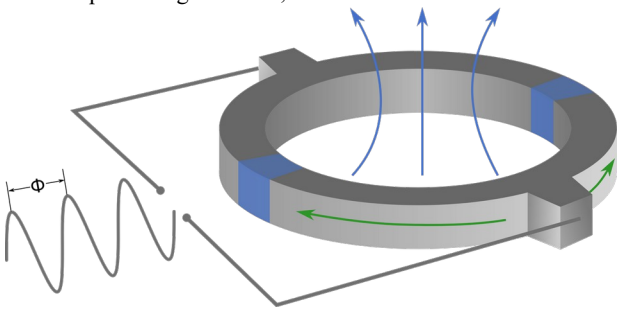

Figure 2: Sketch of a dc SQUID.

- flux quantization: the magnetic flux in the sc ring is quantized with smallest quantity of magnetic flux quantum $\Phi_0 = 2.07 \cdot 10^{-15} Vs$; screening currents flow in the ring,
- Josephson junctions as weak sc section: tunneling described by Josephson effects,
- applied dc bias current which leads to an averaged voltage across the sc ring which depends periodically on the magnetic flux in the sc ring with period of Φ_0; the observed voltage swing is limited by the inductance of the ring; typical inductances of the order of $100\,pH$.

The dc SQUID is driven in a feedback loop, so called flux locked loop or FLL, by a SQUID electronics e.g. [56, 57] in order to linearize its voltage-flux characteristics. This readout circuit results in SQUID being very accurate relative sensors with limitation in ability to track large and/or fast changing signals which is expressed as slew rate.

For highly sensitive magnetometers and gradiometers the limited ring inductance of the SQUID often leads to specific design variants, like multi-loop SQUIDs [58] or flux-transformer SQUID [59] with an inductively coupled large-inductance pickup loop to the SQUID. Flux-transformer SQUIDs are the base of almost all gradiometers introduced hereafter.

Hardware SQUID gradiometers

Hardware SQUID gradiometers provide a well suited sensor technology for application in the Earth's magnetic field. A detailed overview on the theory and implementation of SQUID gradiometers can be found in [60]. Herein, only a short overview will describe the basics.

The hardware SQUID gradiometer facilitates two sc loops which are connected either in series or in parallel. These pickup loops are separated by the base vector $\vec{b}$ (with baseline length $|\vec{b}| = b$) and can have any direction of their sensing area $\vec{A}_i$. Thus, the gradient tensor component B_{ik} which is observed by the gradiometer has to be calculated by

$$B_{ik} = \vec{A} \cdot \hat{B} \cdot \vec{b} \quad \text{with} \quad \vec{A} = \left(-\vec{A}_1 + \vec{A}_2\right)/2 \qquad (2).$$

Therein, $\hat{B}$ presents the $3\,x\,3$ matrix of the first-order magnetic gradient. In practice, two variants of gradiometers are realized. They are illustrated in Fig. 3. Only for very specific applications concentric pickup loops were implemented.

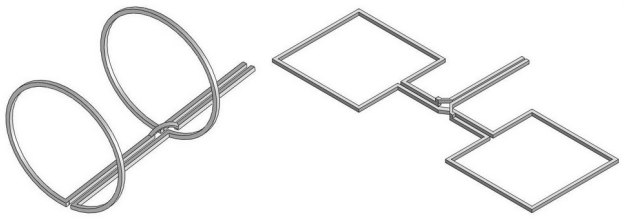

Figure 3: Realization of 1-st order gradiometric pickup loops. An axial and planar-type configuration on the left and right hand side, respectively.

In reality both pickup loop setups can be made either of sc wire, so called wire wound gradiometers [60], or as planar-type pickup loops, typically fabricated on-chip in thin-film superconductor technology.

The response of real gradiometers contains not only the desired tensor components as discussed in eq. (2), but also parasitic contributions caused by fabrication inaccuracies, e.g. difference in the area of the two pickup loops, and the presence of superconducting or conducting material in the vicinity of the gradiometer. These influences are expressed by the balance, often called common-mode [60], and the eddy-current vector:

$$B_{ik} = \vec{A} \cdot \hat{B} \cdot \vec{b} + \sum_{j=1}^{3} \left(\alpha_{ik}\right)_j \cdot B_j + \sum_{j=1}^{3} \left(\varepsilon_{ik}\right)_j \cdot \frac{\partial B_j}{\partial t} \qquad (3).$$

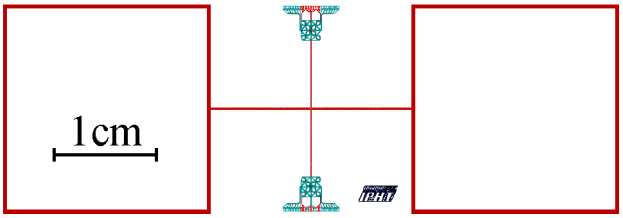

Figure 4: Design of planar-type first-order LTS gradiometer. The antenna loops connected as a figure of eight are placed in the first niobium layer (red) to achieve small parasitic areas.

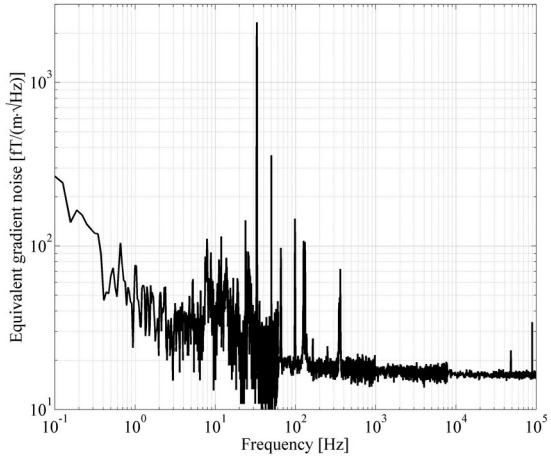

Figure 5: Noise floor measured for a planar-type first-order LTS gradiometer.

The effective volume $V_{eff} = |\vec{A}| \cdot b$ [1] transforms the flux in the SQUID into the amplitude of a magnetic gradient component. The balancing coefficients (α_{ik}) represent the influence of the three orthogonal (parasitic) areas through which the gradiometer still detects a homogenous magnetic field. The coefficients $(\alpha_{ik})_j$ determine the imbalance of a gradiometer, i.e. the inverse of the balance. Conducting material close to the gradiometer induces the eddy current term in eq. (3).

In general, the scheme of parasitic areas and the eddy current term in eq. (3) is universal for any type of gradiometer in each sensor technology, since different scaling factors, misalignment, magnetized and conducting material close to the sensors will cause these effects.

A large variety of hardware SQUID gradiometers have been developed in the past. Those include various wire-wound types e.g. [60]. Planar-type gradiometers are simple to manufacture and this has a great attraction. The most sensitive are still the LTS thin-film gradiometers [61–63]. In Fig. 4 a design and in Fig. 5 a noise spectrum of a highly-symmetric low-noise gradiometer [63] is shown. The gradiometer chip has dimensions of $6.2\,cm \times 2.2\,cm$ and a baseline length of $4\,cm$. The best measured noise inside a superconducting magnetically shielding was about $18\,fT/(m \cdot \sqrt{Hz})$ while a typical sensitivity value is below $50\,fT/(m \cdot \sqrt{Hz})$. For comparison with software gradiometers, one can calculate the sensitivity of one of the gradiometers pickup loop. It amounts to a magnetic field sensitivity of about $18\,fT/(m \cdot \sqrt{Hz}) \cdot b = 0.72\,fT/\sqrt{Hz}$.

With these gradiometers an imbalance of the gradiometers of about $1.3 \ldots 2.1 \cdot 10^{-5}/m$ was achieved. For comparison wire-wound or other planar-type SQUID gradiometers resulted in $2 \cdot 10^{-3}/m$ [64] or $2 \cdot 10^{-4}/m$ [13], respectively. The imbalance of the best HTS gradiometers are typically better than $10^{-4}/m$. The imbalance in practice is increased by thermal cycling of the sensors, use of materials with different thermal expansion coefficients in the sensor mount, or in airborne operation due to vibrations or movements relative to sc or conducting material.

FTMG arrangements using SQUID gradiometer

In order to measure the five independent components of the first-order gradient tensor, various arrangements of the gradiometers were developed:

- Software gradiometers:
  Often eight magnetometers are arranged on rectangular sensor mounts [40], on L-shaped structures [13], or three rotating drums at an angle to measure all tensor components,
- Hardware gradiometers:
  Since mostly planar-type gradiometers are used, a special sensor arrangement is required because the on diagonal components of the tensor B_{ii} could not be measured. One arrangement uses most of the sensors mounted on planes at 90 angles to detect single tensor components and some at $45\,°$ which measure mixtures of the tensor components [13]. The second variant was introduced in [65]. According to this patent the gradiometers are mounted on the surfaces of a five- or six-sided frustum of a pyramid. The side walls are on a specific angle to the base of the frustum. One example is shown in Fig. 6.
  Both variants require decomposing the mixed tensor components into the individual tensor components. This un-mixing procedure requires simply solving a linear system of equations where the coefficients correspond to the geometry of the gradiometer arrangement [63, 66].

[1] For SQUIDs an effective area A_{eff} instead of $|\vec{A}|$ has to be used which are caused by transformation losses.

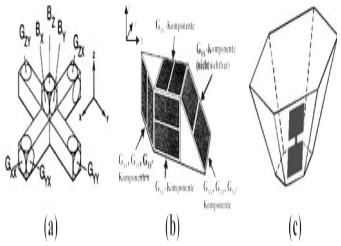

Figure 6: Gradiometer arrangement for FTMG. One gradiometer is illustrated by the gray shaded shape.

Mobile operation of SQUIDs

The magnetically unshielded operation of SQUID gradiometers provides a few challenges [67] which include:

1) SQUID as magnetic flux detector:
   - change of working point due to flux trapping in Josephson junctions; heating above critical temperature often solves the issue,
   - magnetic flux creeping in sc structures causes low frequency noise; heating above critical temperature often resolves this issue,
   - loss of flux lock due to RF or large/fast signal interference which is reduced by applying RF screening,
   - magnetic hysteresis caused by entry of magnetic flux into the sc structures especially if the gradiometers are rotated in the Earth's magnetic field; narrow sc structures with deep, smooth edge profiles help to reduce the hysteresis.
2) The ***imbalance*** should be as small as possible for mobile gradiometers. It could be further enhanced by using reference magnetometers using offline compensation. Thus, high linearity and small delays between the sensor signals are required. A further reduced imbalance by a factor of more than 50 has been demonstrated for planar-type LTS gradiometers [63].
3) Higher imbalance of the gradiometer and larger regional gradients require larger DNR as discussed earlier. Typical values for the DNR are given for instance in [15].
4) Magnetic noise due to e.g. spherics with wavelength of larger than $100\,km$ do not cause signals for short baseline gradiometers. Thus, no base station is required.
   But, in case of magnetic storms the slew rate of the FLL could be exceeded as well as the induced magnetization of underlying material could change. It is not advisable to perform magnetic surveys during such storms.
5) The whole environment has to be designed for low noise gradiometer operation. This includes platform noise caused by magnetized or electrically conducting material close to the sensors. Also all electronic equipment has to be at sufficient distance from the gradiometers. This can easily be ensured by utilizing towed operations where the distance between sensor and towing vehicle can be chosen. Other platforms like boom mounts or inside unmanned aerial, sub- or marine vehicles do not allow reducing the interferences by increasing distance to the sensors. The use of reference sensors e.g. fluxgates helps to further remove noise from the sensor signals, e.g. OPM in helicopter boom operation or other interference signals helping to actively reduce the platform noise.
6) Mechanical considerations: Relative movement of the gradiometers against magnetized or electrically conducting material has to be prevented during operation. There are two options chosen in the past: The sensors could be rigidly and reliable mounted against other system components, or they can be placed on a damped gimbal. Special compensation algorithms are required for gimbal-mounted instruments due to disturbances caused by relative motion.
   For field operation, the simplest cooling of SQUIDs is to immerse them in cryogenic liquids. But, bubbles and motion of liquid in the cryostat will cause additional noise due to mechanical impact and magnetic signal especially in case of contamination of liquid nitrogen with oxygen. This can be prevented by sloshing plates or other means.
7) Other required system components:
   Important instrument components are the ADCs which digitize the analogue SQUID signals at very high precision. State of the art ***24 bit ADC***s provide very low noise, extremely low drift, high dynamic range and linearity.
   More important is a very high precision inertial measurement system (***IMU***) and related processing [68] for calculating the attitude, i.e. the Euler angles. They are applied in processing to reduce motion noise. While for sensitive magnetometers an extreme resolution is required, for FTMG an accuracy of about $0.1\,°_{RMS}$ is often sufficient to reduce the sensitivity for rotations and to transform the MGT from the body into the Earth centered-Earth fixed coordinate system (ECEF).
   Typically altitude and thus pressure changes cause temperature fluctuations in the cryogenic liquid. Therefore, a nonmagnetic pressure regulator is often used in SQUID instruments to keep the pressure and temperature in the cryostat constant.

PROCESSING OF FTMG DATA

In the last couple of years significant progress has been made with the processing of FTMG data [25, 69]. The main developments are emphasized below and the specific processing steps required for SQUID based FTMG are discussed:

Synchronization of data streams

FTMG instruments often provide data streams with different time bases e.g. GPS, IMU, ADC stream of magnetometers, which have to be synchronized to a common time base.

De-Fluxing

This procedure is only required for the SQUID sensor signals since RF interference or other strong/fast signals may unlock and relock the system which results in integer voltage jumps which

correspond to multiple of a magnetic flux quantum in the periodic SQUID characteristics.

This process needs to identify sudden voltage jumps of a specific height. This could be difficult when e.g. crossing power lines and large amplitude $50/60\ Hz$ contributions are overlaid in the signal. Thereafter, the step has to be removed by subtracting an estimated multiple of flux quanta and then interpolating the time series at this time stamp.

An advanced algorithm which uses Wavelet for detection and subtraction of an idealized step response including the Gibbs ringing was already introduced [70].

Magnetometer calibration

Since SQUIDs are relative sensors, this step is required to compensate for scaling and misalignment error as well as offset in the reference magnetometer signals. Two approaches [71, 72] are applied and discussed in [66] which result in good quality magnetometer signals.

Balancing/Compensation

This process intends to further reduce the influence of the homogeneous magnetic field onto the gradiometer signals. Thus, from the measurements of the tensor components and the reference magnetometers the proportionality factors of the homogeneous part, the so called balancing coefficients $\left(\alpha_{ik}\right)$, will be estimated. This can be done by least squares (LSQ) or optimization or singular value decomposition (SVD) methods. For the processing of the JESSY STAR instrument data a new balancing method has been introduced. It combines a robust LSQ fitting with a regional balancing in time and frequency domain: part of the time series with strong magnetic anomalies and low-frequency components are cut out for estimation of the $\left(\alpha_{ik}\right)$.

Since the balancing procedure takes the three orthogonal magnetic field components into account, it is mixed with the so called aircraft compensation where the sensors are in an environment with magnetisable and conducting materials which have an influence on the magnetic field vector too. These compensation methods go back to Leliak et al. [73]. First approaches for MGT surveys are introduced in [74].

Unmixing

In this step, the mixed tensor components measured e.g. by planar gradiometers are decomposed into pure tensor components in a Cartesian frame e.g. [65]. If each tensor component is purely measured by the FTMG instrument this step is not required.

Rotation into ECEF

The MGT subsequently is rotated into an ECEF frame by the mathematical operation $\left(B_{ij}\right)_{NED}=\left(D^{B}{}_{NED}\right)^{T}\cdot\left(B_{ij}\right)_{B}\cdot D^{B}{}_{NED}$. The $\left(B_{ij}\right)_{B}$ and $\left(B_{ij}\right)_{NED}$ are the MGT in body and in North-East-Down (NED) frame, respectively. The rotations are done by the according matrices $D^{B}{}_{NED}$ which contain three rotations by the Euler angles. A detailed description could be found in [66].

Compensation

This step is currently combined with the balancing of the gradiometer signals. However, sometimes a procedure for removal of anthropogenic signals is applied to the MGT data. With an original sampling rate of $1\,kHz$ it is possible to extract the $50\,Hz$ and $16\frac{2}{3}\,Hz$ frequency components from individual sensor signals providing information about e.g. power lines and railways. In combination with the operator's notes during survey and the joint assessment of the magnetic maps with ortho-photographs such anomalies could easily be identified and removed from the magnetic signals.

Microlevelling

After the processing often a stripe-shaped noise texture remains in the MGT components. The source of these corrugations are either numerical inaccuracies of balancing and magnetometer calibration which lead to an imperfect deconvolution of rotational noise from the gradiometer signals as well as small differences in the flight altitudes between adjacent profile lines. Furthermore, different climbing and descending behavior at hill ridges lead to slightly different distances to the magnetic sources depending on flight direction.

Usually these errors are fixed using FFT decorrugation [75], where an error grid by suitable bandpass and directional cosine filters is calculated and subtracted or median filters [76–78]. But, these approaches were found to perform insufficient decorrugation and may lead to the removal of magnetic anomalies from the magnetic maps. Furthermore, symmetry and tracelessness of the MGT is not preserved.

Therefore, a new moving median filter approach was introduced: With a Weiszfeld median filter [79], tensorial consistency is provided and an elliptical search window preserves the shape and amplitude of the magnetic anomalies.

Transformations: Hilbert and Hilbert-like

Due to restrictions regarding the accuracy of the IMU, the Euler angles are not accurate enough to use them for a rotation of the magnetic field vector into the ECEF frame. Hence, suitable approaches to circumnavigate it are introduced in [80]: Firstly, the vertical gradient components could be integrated into the corresponding magnetic field vector components in Fourier space. This resembles so called Hilbert transforms [81–84] with the capability of measuring true gradients. Afterwards, the homogeneous magnetic field contribution are calculated either using the IGRF [16] or the HDGM [85]. This contribution is summed up with the vector anomalies.

Secondly, the entire MGT could be transformed into the magnetic field vector which offers a better resolution of the magnetic field vector anomalies by including horizontal gradient information.

Thirdly, the approach of [86], which transforms the TMI into the magnetic field vector, is used with the calibrated magnetometer signals. This step gains the long-wavelength structures in the 2D magnetic field component maps which are not covered by the magnetic gradients.

Finally, the combination of the last two approaches on a wavelength-dependent basis will be used for a proper reconstruction of the magnetic field vector.

Tensor interpolation and gridding

In order to preserve the MGT properties, special attention must be paid for interpolation and gridding of the 2D tensor component maps. Most of the common tools, i.e. Inverse Distance Weighting, Delaunay triangulation, Minimum Curvature methods [87] and Kriging, are not designed for tensor interpolation but it is possible to modify them for tensorially consistent operation. A promising way relies on a principal axis transformation of the MGT into its structural, represented by the rotationally invariant Eigenvalues, and its rotational part described by rotation matrices consisting of the Eigenvectors. Whereas the Eigenvalues could be interpolated and gridded with classical linear operations, the representation of the rotational part is done in quaternions. The interpolation of the quaternions laying along geodesics of S^3 by so-called spherical linear interpolation, or "SLERP" [88, 89].

Inversion and Interpretation

With the final step of processing the subsurface distribution of the sources causative for MGT anomalies and estimates of the magnetic susceptibility or magnetization can be derived using 3D inversion. A few algorithms exist for the inversion of FTMG data: Prominently, the groups at the University of Utah and TechnoImaging LLC [90, 91], pbEncom® (ModelVision Pro), Intrepid Geophysics (3D GeoModeller), and recently Geosoft® VOXI all include MGT inversion.

Inversion is performed as an iterative update of a susceptibility/magnetization model controlled by first-order model gradients, using a suitable step length, regularization and appropriate depth weighting. The two most familiar iterative solvers are regularized Newton [92–94] and conjugate gradient [90] algorithms. Regularization is highly important as potential field inversion is generally ambiguous. Often smoothing inversions with a minimum norm stabilizer are used, but smooth inversions rarely match the true geology where discontinuous boundaries are common. Therefore, focusing inversion with minimum support functionals [90] become also important as they can reproduce sharp boundaries. In contrast to TMI inversion, the depth weighting must be controlled [93] to derive depth estimates as well as geometric and magnetic inclination values.

Recent advances, i.e. fuzzy c-means clustering [95], gramian constraints reflecting the symmetries of the magnetization vector [96, 97] and different parametrization of the magnetization vector [98] help to perform more realistic and constrained inversion and open a path for a suitable assessment of remanent magnetization from the inversion results. Incorporating these options into the inversion is highly beneficial for mineral exploration.

The authors initiated their own implementation of a 3D FTMG magnetic vector inversion (MVI) algorithm. Besides the mentioned state-of-art it incorporates a better adaption to the topography and a combination of four different factors strongly reducing the computational time: Firstly, intrinsic symmetries inside the forward modelling operators are exploited. Secondly, a vectorization over the whole model space is used. Thirdly, the forward calculation is parallelized over all observation points. Finally with the footprint approach [99], reflecting the spatial decay behavior of the MGT, the FTMG inversion runs many times faster than the single-channel TMI inversion and provides a higher accuracy.

JESSY STAR – A FTMG INSTRUMENT

System setup for towed airborne operation

The JESSY STAR system uses six first-order planar-type SQUID gradiometers [62]. To further enhance the balance by compensation, magnetic field components are also measured with three separate orthogonal lower sensitivity SQUID magnetometers with noise figures of about $7\ pT/\sqrt{Hz}$ [100]. All SQUIDs are immersed in liquid helium using a plastic cryostat inside a nonmagnetic aerodynamically shaped shell (Fig. 7).

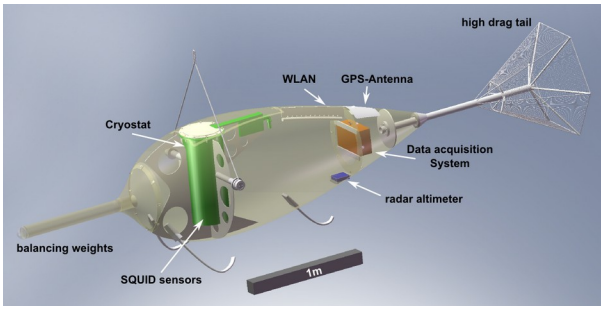

Figure 7: Towed bird of JESSY STAR (description in text).

Figure 8: JESSY STAR (6th generation) during take-off.

The SQUID signals are digitized using 24 bit ADCs in the data acquisition system (DAS) with a sampling rate of $1\,kHz$ which is in post-processing decimated (lowpass filtering to prevent aliasing and then downsampling the signal) to $10\,Hz$. The DAS also digitizes other reference signals like temperatures, currents, fluxgates or OPM. Position and attitude are recorded using a differential GPS receiver (Novatel OEM628) and a high-resolution inertial unit to estimate attitude in terms of Euler angles. Data are transferred via a wireless connection to a laptop on board of the helicopter for system control. All DAS components are specifically designed not to cause magnetic disturbances. The system in Fig. 7 is mounted in a nonmagnetic shell which is balanced using ballast weights in the nose and the high drag tail in the back. The bird is towed at about $100\,km/h$ by a helicopter (AS350 B2 or BGR's Sikorsky S-76B in Germany) using a $30\,m$ long nylon (Dyneema™) rope (Fig. 8) with ground clearance of about $30\,m$.

Recently, in [101] a FTMG system was introduced with a towed bird which is very similar to the older fourth generation JESSY STAR instrument which was used in the example presented in the next section. The processing stream of the acquired data was partially described in the previous section. The full workflow is described in [66].

Example airborne operation

Since 2004 airborne survey operations with different system generations of JESSY STAR were undertaken. Some examples are presented in [69, 100, 102]. Herein, the focus is laid on an example from the Bushveld complex in the Republic of South Africa [66] which was already published in [102], see Fig. 9. The survey was conducted with the fourth generation system in September 2006 [100] focusing on the Merensky Reef and UG2 layer (platinum and chromitite) in the Bushveld Igneous Complex. The aim of the survey was to resolve the various dolerite dyke swarms [103]. The airborne operation was undertaken on a draped surface (clearance in avg. $77\,m$) comprising 141 lines at $50\,m$ line separation over some steep topographical changes.

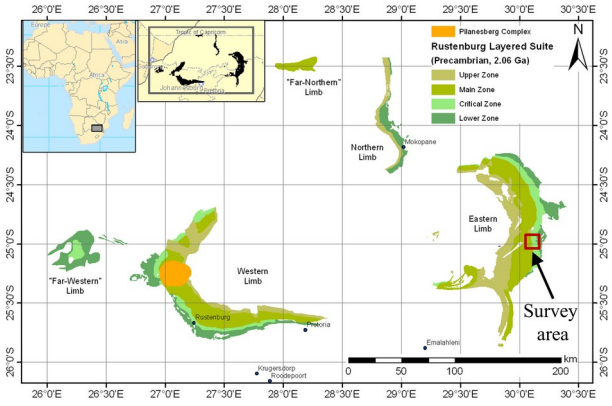

Figure 9: Survey area in the Bushveld complex.

The data were recently re-processed using the latest processing tools described above. The tensor components are shown in Fig. 10. In each of the various tensor components, acting as directional filters, the expected geological structures could be well observed, see Fig. 11. Using the 3D inversion algorithms including tetrahedral discretization, misfits of about $9.1\,\%$ in typically 25 iterations (about $1.600\,s$ per iteration) were achieved [66]. Since mainly induced magnetization was found in the full MVI, only the downward magnetization will be depicted in Fig. 12. The focusing inversion of the FTMG data was very robust against regularization and discretization. Compared to other inversion variants, sharply delineated geological structures are observable in Fig. 12 which is a geologically plausible result. Dolerite dykes with a width of $25\ldots75\,m$ at the surface are clearly resolved from surface to a depth of about $300\,m$. This is in very good agreement with ground-truth data presented in [103].

Case studies on the extraction of remanence indicators [104] are ongoing.

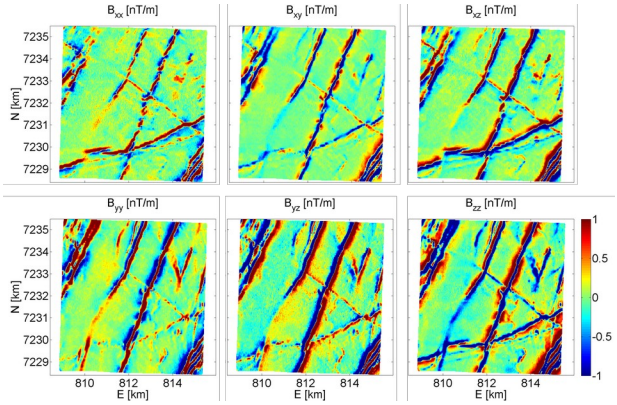

Figure 10: Survey area.

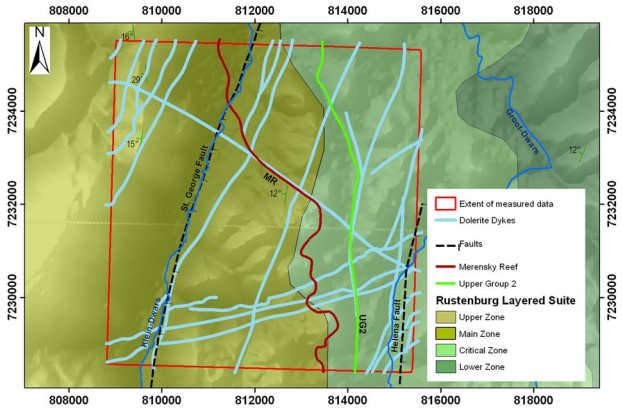

Figure 11: Geological setting of study area (Council for Geoscience South Africa. 1:1,000,000 Geological Data 2012).

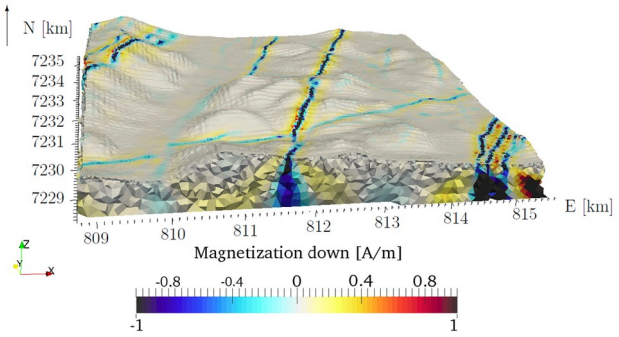

Figure 12: Downward component of magnetization vector derived by the inversion for the survey area.

REVIVAL OF VECTOR MAGNETOMETRY

As discussed earlier, the signal of highly sensitive magnetometers in mobile operation in the Earth's magnetic field exceeds the *DNR* of all commercially available ADCs substantially. Thus, innovative technologies are required to overcome this hurdle. The undisturbed periodic SQUID characteristic provides a base for new vector magnetometers. There are several possible options including:

- flux-quanta counting electronics e.g. [38, 39, 65],
- SQUID cascade magnetometers [105] or
- digital e.g. [106] and hybrid digital SQUIDs e.g. [107].

More details can be found in Chwala et al. in this publication.

These concepts may allow the construction of new FTMG instruments to create a high resolution 3D vector magnetometer. Thus, on the one hand the long wavelength geological structures and on the other hand conductive sub-surface structures using passive electromagnetics will in future also be explorable by the same instrument.

CONCLUSIONS

Airborne full tensor gradiometry has successfully proven its potential as an important exploration tool for natural gas and oil,

coal, mineral resources, geotechnical sources such as pipes, UXO's as well as for other geoscientific and archaeological projects. Amongst the various available sensor technologies, SQUID full tensor magnetic gradiometers currently define the state of the art. Also based on the SQUID technology a new FTMG instrument will be in future feasible which incorporates a highly sensitive 3D vector magnetometer together with the gradiometers. But, this will require further development of new technologies.

Within the next few years, new non-cryogenic sensor technologies which were already demonstrated may enter the market and will generate exciting opportunities for the magnetic exploration method.

ACKNOWLEDGEMENTS

We thank Anglo American, De Beers for their continuous funding and Spectrem Air Ltd. for their support with the survey operation.

Part of this work was done within the INFLUINS project by the German Federal Ministry of Education and Research (BMBF grant No. 03IS2091). We thank all involved partners of the INFLUINS network, especially the BGR in Hannover, Germany.

We thank Michael S. Zhdanov and Martin Čuma for providing access to their inversion code as well as supporting the working stay of one colleague in Utah of the INFLUINS network, especially the BGR in Hannover, Germany.

We thank Michael S. Zhdanov and Martin Čuma for providing access to their inversion code as well as supporting the working stay of one colleague in Utah.

REFERENCES

[1] Hinze W J, Saad A H and Frese R von 2013 *Gravity and magnetic exploration: Principles, practices, and applications* (Cambridge: Cambridge University Press)
[2] Nabighian M N and Asten M W 2002 *Geophysics* **67** 964–78
[3] Nabighian M N, Grauch V J S, Hansen R O, LaFehr T R, Li Y, Peirce J W, Phillips J D and Ruder M E 2005 *Geophysics* **70** 33
[4] Vallée M A, Smith R S and Keating P 2011 *Geophysics* **76** W31-W50
[5] Ludwig K-H and Schmidtchen V 1997 *Propyläen Technikgeschichte <2>: Metalle und Macht ; 1000 bis 1600* 1990th edn (Berlin: Propyläen)
[6] Gordon D and Brown R 1972 *IEEE Trans. Magn.* **8** 76–82
[7] Ripka P 1992 *Sensors and Actuators A: Physical* **33** 129–41
[8] Ripka P 2003 *Sensors and Actuators A: Physical* **106** 8–14
[9] Grosz A, Haji-Sheikh M J and Mukhopadhyay S C (eds) 2017 *High Sensitivity Magnetometers (Smart Sensors, Measurement and Instrumentation* vol 19*)* (Cham, s.l.: Springer International Publishing)
[10] Boll R and Overshott K J 2008 *Sensors: Magnetic Sensors (Sensors* vol 5*)* (Hoboken: Wiley-VCH)
[11] Lenz J and Edelstein S 2006 *IEEE Sensors J.* **6** 631–49
[12] Tumanski S 2007 *Meas. Sci. Technol.* **18** R31-R46
[13] Clem T R, Kekelis G J, Lathrop J D, Overway D J and Wynn W M 1996 Superconducting Magnetic Gradiometers for Mobile Applications with an Emphasis on Ordnance Detection *SQUID Sensors: Fundamentals, Fabrication and Applications* ed H Weinstock (Dordrecht: Springer Netherlands) pp 517–68
[14] Chwala A, Stolz R, IJsselsteijn R, Schultze V, Ukhansky N, Meyer H-G and Schüler T 2001 *Supercond. Sci. Technol.* **14** 1111–4
[15] Clem T R, Foley C and Keene M N 2005 SQUIDs for Geophysical Survey and Magnetic Anomaly Detection *The SQUID Handbook, Vol.2: Applications of SQUIDs and SQUID Systems* ed J Clarke and A I Braginski (Weinheim, Chichester: Wiley-VCH; John Wiley [distributor],) pp 482–543
[16] Thébault E *et al* 2015 *Earth Planet Sp* **67** 67–79
[17] Maus S, Nair M C, Poedjono B, Okewunmi S, Fairhaid D, Barckhausen U, Milligan P R and Matzka J 2013 High-Definition Geomagnetic Models: A New Perspective for Improved Wellbore Positioning *IADC/SPE Drilling Conference and Exhibition IADC/SPE Drilling Conference and Exhibition (San Diego, California, USA, 2012-03-06)* (Society of Petroleum Engineers) 151436-1–15
[18] Scintrex Ltd. 2017 *CS-3 CESIUM MAGNETOMETER: High Resolution Magnetics* http://scintrexltd.com/dat/content/CS-3.pdf
[19] Budker D and Jackson Kimball D F 2013 *Optical Magnetometry* (Cambridge: Cambridge University Press)
[20] Kominis I K, Kornack T W, Allred J C and Romalis M V 2003 *Nature* **422** 596–9
[21] Dang H B, Maloof A C and Romalis M V 2010 *Appl. Phys. Lett.* **97** 151110
[22] Schultze V, Schillig B, IJsselsteijn R, Scholtes T, Woetzel S and Stolz R 2017 *Sensors (Basel, Switzerland)* **17** 561-1 - 561-19
[23] Schmidt P W and Clark D A 2006 *The Leading Edge* **25** 75–8
[24] Pedersen L B and Rasmussen T M 1990 *Geophysics* **55** 1558–66
[25] FitzGerald D J and Holstein H 2006 *The Leading Edge* **25** 87–94
[26] Wynn W, Frahm C, Carroll P, Clark R, Wellhoner J and Wynn M 1975 *IEEE Trans. Magn.* **11** 701–7
[27] Fromm W E 1952 The Magnetic Airborne Detector *(Advances in Electronics and Electron Physics* vol 4*)* (Elsevier) pp 257–99
[28] Wyckoff R D 1948 *Geophysics* **13** 182–208
[29] Morris R M and Pedersen B O 1961 *Review of Scientific Instruments* **32** 444–8

[30] Gamey T J, Doll W E, Beard L P and Bell D T 2004 *JEEG* **9** 115–25
[31] Wiegert R, Oeschger J and Tuovila E 2007 Demonstration of a Novel Man-Portable Magnetic STAR Technology for Real Time Localization of Unexploded Ordnance *Oceans 2007 (Vancouver, BC, Canada)* pp 1–7
[32] Engels M, Barckhausen U and Gee J S 2008 *Geophysical Journal International* **172** 115–29
[33] Wickerham W E 1954 *Geophysics* **19** 116–23
[34] Hogg S 2004 *First Break* **22 (7)** 59–65
[35] Koch R H, Rozen J R, Sun J Z and Gallagher W J 1993 *Appl. Phys. Lett.* **63** 403–5
[36] Humphrey K P, Horton T J and Keene M N 2005 *IEEE Trans. Appl. Supercond.* **15** 753–6
[37] Ludwig C, Kessler C, Steinforc A J and Ludwig W 2001 *IEEE Trans. Appl. Supercond.* **11** 1122–5
[38] Zimmermann E *et al* 1997 HTS-SQUID Magnetometer with Digital Feedback Control for NDE Applications *Review of Progress in Quantitative Nondestructive Evaluation: Volume 16A* ed D O Thompson and D E Chimenti (Boston, MA: Springer US) pp 2129–35
[39] Vrba J *et al* 2000 143 Channel Whole-Cortex MEG System *Biomag 96* ed C J Aine *et al* (New York, NY: Springer New York) pp 138–41
[40] Tristan Technologies 2017 *T877 Tensor Gradiometer* http://tristantech.com/pdf/T877datasheet.pdf
[41] Tilbrook D L 2004 *Physica C: Superconductivity* **407** 1–9
[42] Tilbrook D L 2009 *Supercond. Sci. Technol.* **22** 75002
[43] Schmidt P W, Clark D A, Leslie K, Bick M, Tilbrook D and Foley C 2004 *Exploration Geophysics* **35** 297–305
[44] Colombo A P, Carter T R, Borna A, Jau Y-Y, Johnson C N, Dagel A L and Schwindt P D D 2016 *Optics Express* **24** 15403–16
[45] Jeske J, Cole J H and Greentree A D 2016 *New J. Phys.* **18** 13015
[46] Acosta V M 2011 Optical Magnetometry with Nitrogen-Vacancy Centers in Diamond *PhD Thesis* University of California, Berkeley, USA
[47] Blakley S M, Fedotov I V, Kilin S Y and Zheltikov A M 2015 *Optics letters* **40** 3727–30
[48] Blakley S M, Fedotov I V, Amitonova L V, Serebryannikov E E, Perez H, Kilin S Y and Zheltikov A M 2016 *Optics letters* **41** 2057–60
[49] Wood A A, Bennie L M, Duong A, Jasperse M, Turner L D and Anderson R P 2015 *Phys. Rev. A* **92** 053604 1-6
[50] Veryaskin A V 2001 *Sensors and Actuators A: Physical* **91** 233–5
[51] Sunderland A, Ju L, Blair D G, McRae W and Veryaskin A V 2009 *The Review of scientific instruments* **80** 104705
[52] Buckel W and Kleiner R 2004 *Superconductivity* (Weinheim, Germany: Wiley-VCH Verlag GmbH)
[53] Clarke J and Braginski A I (eds) 2004 *The SQUID Handbook* (Weinheim, FRG: Wiley-VCH Verlag GmbH & Co. KGaA)
[54] Seidel P (ed) 2015 *Applied superconductivity: Handbook on devices and applications (Encyclopedia of Applied Physics)* (Weinheim: Wiley-VCH)
[55] Jaklevic R, Lambe J, Silver A and Mercereau J 1964 *Phys. Rev. Lett.* **12** 159–60
[56] Oukhanski N, Stolz R, Zakosarenko V and Meyer H-G 2002 *Physica C-Superconductivity and Its Applications* **368** 166–70
[57] Oukhanski N, Stolz R and Meyer H-G 2006 *Applied Physics Letters* **89**
[58] Drung D, Knappe S and Koch H 1995 *Journal of Applied Physics* **77** 4088–98
[59] Warzemann L, Schambach J, Zakosarenko V, Bluethner K, Berthel K H, Stolz R and Weber P 1995 *Applied Superconductivity 1997, Vol 1: Small Scale and Electronic Applications* **148** 1613–6
[60] Vrba J 1996 SQUID Gradiometers in Real Environments *SQUID Sensors: Fundamentals, Fabrication and Applications (NATO ASI Series)* ed H Weinstock (Springer Netherlands) pp 117–78
[61] Cantor R, Hall A and Matlachov A 2006 *J. Phys.: Conf. Ser.* **43** 1223–6
[62] Stolz R, Zakosarenko V M, Fritzsch L, Oukhanski N and Meyer H G 2001 *IEEE Transactions on Applied Superconductivity* **11** 1257–60
[63] Stolz R 2006 *Supraleitende Quanteninterferenzdetektor-Gradiometer-Systeme für den geophysikalischen Einsatz: PhD Thesis* (Ilmenau: Isle)
[64] Clem T R 1995 *IEEE Trans. Appl. Supercond.* **5** 2124–8
[65] Eschner W and Ludwig W 1995 Planar gradiometers arranged on non-parallel surfaces for determination of a gradient tensor of a magnetic field *US5469056 A*
[66] Schiffler M 2017 Processing, Analysis and Inversion of Full Tensor Magnetic Gradiometry Data *PhD Thesis* Friedrich Schiller University Jena, Germany
[67] Stolz R 2015 9.3.4 SQUIDs in Geophysics *Applied Superconductivity: Handbook on Devices and Applications* ed P Seidel (Wiley-VCH) pp 1020–41
[68] Shin E H and El-Sheimy N 2004 *Aided Inertial Navigation System (AINS™) Toolbox for MatLab™ Software: INS/GPS integration software* (Mobile Multi-Sensors Systems R&D group, University of Calgary, Canada, http://mms.geomatics.ucalgary.ca/Research/research.htm)
[69] FitzGerald D J, Argast D, Holstein H and Paterson N R 2010 Full Tensor Magnetic Gradiometry Processing and Interpretation Developments *EGM 2010 International Workshop* pp 1–6
[70] Schönau T, Schneider M, Schiffler M, Schmelz M, Stolz R and Meyer H-G 2013 *Meas. Sci. Technol.* **24** 125004
[71] Olsen N, Risbo T, Brauer P, Merayo J, Primdahl F and Sabaka T J 2001 In-flight calibration methods used for the Ørsted mission *Ground and In-Flight Space Magnetometer Calibration Techniques,* ed A Balogh and F Primdahl pp 1–13
[72] Merayo J M G, Brauer P, Primdahl F, Petersen J R and Nielsen O V 2000 *Meas. Sci. Technol.* **11** 120–32
[73] Leliak P 1961 *IRE Transactions on Aerospace and Navigational Electronics* **ANE-8 (3)** 95–105
[74] FitzGerald D J and Perrin J 2015 Magnetic Compensation of Survey Aircraft; a poor man's approach and some re-imagination *14th International Congress of the Brazilian Geophysical Society & EXPOGEF, Rio de Janeiro, Brazil, 3-6 August 2015 14th International Congress of the Brazilian Geophysical Society & EXPOGEF, Rio de Janeiro, Brazil, 3-6 August 2015 (Rio de Janeiro, 03 August*

to 06 August) ed R A R Fernandes (Brazilian Geophysical Society) pp 741–4
[75] Valleau N 2004 *Microlevelling using FFT Decorrugation*
[76] Mauring E and Kihle O 2000 *Micro-levelling of aeromagnetic data using a moving differential median filter* (Report 2000.053, Geological Survey of Norway)
[77] Mauring E, Beard L P, Kihle O and Smethurst M A 2002 *Geophys Prospect* **50** 43–54
[78] Mauring E and Kihle O 2006 *Geophysics* **71** L5-L11
[79] Weiszfeld E 1937 *Tôhoku Mathematical Journal* **43** 355–86
[80] Schiffler M, Queitsch M, Stolz R, Meyer H-G and Kukowski N 2017 *Geophys Prospect* **6** 76–90
[81] Nabighian M N 1972 *Geophysics* **37** 507–17
[82] Nabighian M N 1984 *Geophysics* **49** 780–6
[83] Nelson J B 1986 *Geophysics* **51** 1014–5
[84] Nelson J B 1988 *Geophysics* **53** 957–66
[85] Maus S 2010 An ellipsoidal harmonic representation of Earth's lithospheric magnetic field to degree and order 720 *G3: Geochemistry, Geophysics, Geosystems AGU (2010)* vol 11 ed AGU and the Chemichal Society pp 1–12
[86] Lourenco J S and Morrison H F 1973 *Geophysics* **38** 359–68
[87] Briggs I C 1974 *Geophysics* **39** 39–48
[88] Shoemake K 1985 Animating rotation with quaternion curves *12th annual conference of the Association of Computing Machinery (ACM) (San Francisco)* 19 (3) pp 245–54
[89] Kuipers J B 2002 *Quaternions and rotation sequences: A primer with applications to orbits, aerospace, and virtual reality* (Princeton, N.J., Oxford: Princeton university press)
[90] Zhdanov M S 2002 *Geophysical inverse theory and regularization problems (Methods in geochemistry and geophysics* vol 36*)* (Amsterdam and Oxford: Elsevier Science)
[91] Zhdanov M S, Cai H, Fatehi Marji M and Wilson G A 2012 *Journal of Geology & Geosciences* **01** 1000104-1-5
[92] Li Y and Oldenburg D W 1996 *Geophysics* **61** 394–408
[93] Li Y and Oldenburg D W 2000 *Geophysics* **65** 540–52
[94] Li Y and Oldenburg D W 2003 *Geophysical Journal International* **152** 251–65
[95] Li Y and Sun J 2014 Total magnetization vector inversion using guided fuzzy c-means clustering *SEG Technical Program Expanded Abstracts 2014 (Denver, Colorado, 26 October to 31 October)* ed B Birkelo pp 1285–90
[96] Zhdanov M S, Gribenko A and Wilson G 2012 *Geophys. Res. Lett.* **39** L09301 1–7
[97] Zhu Y, Zhdanov M S and Čuma M 2015 Inversion of TMI data for the magnetization vector using Gramian constraints *SEG Technical Program Expanded Abstracts 2015 (New Orleans, Louisiana, 18 October to 23 October)* ed R V Schneider pp 1602–6
[98] Lelièvre P G and Oldenburg D W 2009 *Geophysics* **74** L21-L30
[99] Čuma M, Wilson G A and Zhdanov M S 2012 *Geophys Prospect* **60** 1186–99
[100] Stolz R, Zakosarenko V, Schulz M, Chwala A, Fritzsch L, Meyer H-G and Köstlin E O 2006 *The Leading Edge* **25** 178–80
[101] Qiu L, Rong L, Wu J, Wang Y, Zhang G, Wang S and Xie X 2016 Development of a squid-based airborne full tensor gradiometers for geophysical exploration *SEG Technical Program Expanded Abstracts 2016 (Dallas, Texas, 16 October to 21 October)* ed C Sicking and J Ferguson pp 1652–5
[102] Rompel A K K 2009 *11th SAGA Biennial Technical Meeting and Exhibition* 39–42
[103] Holland M 2014 *Der Brochen Project - Groundwater Investigation and Model Report* (Pretoria, South Africa: SRK Consulting South Africa (Pty) Ltd)
[104] Queitsch M 2016 Modeling and Inversion of airborne Full Tensor Magnetic Gradiometry Data in the Thuringian Basin and Forest *PhD Thesis* Friedrich Schiller University Jena, Germany
[105] Schoenau T, Schmelz M, Zakosarenko V, Stolz R, Meyer M, Anders S, Fritzsch L and Meyer H-G 2013 *Superconductor Science & Technology* **26 (3)** 035013-1 - 035013-7
[106] Haverkamp I, Wetzstein O, Kunert J, Ortlepp T, Stolz R, Meyer H-G and Toepfer H 2012 *Superconductor Science & Technology* **25 (6)** 065012-1 - 065012-8
[107] Reich T, Febvre P, Ortlepp T, Uhlmann F H, Kunert J, Stolz R and Meyer H-G 2008 *Journal of Applied Physics* **104 (2)** 024509-1 - 024509-10